Electronic and Geometric Structure of a Trinuclear Mixed-Valence Copper(II,II,III) Cluster

David E. Root, Mark J. Henson, Tim Machonkin, Pulakesh Mukherjee, T. D. P. Stack,* and Edward I. Solomon*

Contribution from the Department of Chemistry, Stanford University, Stanford, California 94305

Received October 9, 1997

Abstract: The four-electron reduction of dioxygen to water by trinuclear copper clusters is of great biological significance. Recently we reported the crystal structure of a trinuclear model complex in which the three coppers provide the four electrons necessary to fully reduce dioxygen, generating two μ_3-oxo bridges. This complex is best described as a localized, mixed-valence Cu(II,II,III) system which has C_{2v} effective symmetry. The magnetic properties of this trinuclear cluster have been investigated by MCD and SQUID magnetic susceptibility. The two Cu(II) ions are found to be ferromagnetically coupled with a triplet/singlet splitting of 14 cm^{-1}. Density functional calculations reproduce these geometric, electronic, and magnetic properties of the trinuclear cluster and provide insight into their origin. Since the trinuclear copper complex has a 3+ charge, the Cu_3O_2 core is one electron too oxidized to permit each atom to be in a preferred oxidation state (2+ for Cu and 2− for O). The extra hole in this highly oxidized Cu_3O_2 cluster is found to be localized on one Cu, which is therefore a Cu(III) ion, rather than on an O ligand (which would then be an oxyl) due to the strong stabilization of the oxo valence orbitals which derives from bridging to the Cu(II) centers. The communication between the coppers is weak, as it involves superexchange through the oxo bridges which provide nearly orthogonal orbital pathways between the copper ions. This leads to a ferromagnetic interaction between the two Cu(II) ions and weak electronic coupling between the Cu(III) and the Cu(II) ions. In the idealized D_{3h} high symmetry limit which would be the favored geometry in the case of complete electronic delocalization, the triplet ground state is orbitally degenerate and subject to a large Jahn−Teller distortion [E′ ⊗ e′] toward the observed C_{2v} structure. This combination of a large Jahn−Teller distortion and weak electronic coupling leads to localization of the Cu(III) on one metal center.

Introduction

The binding and activation of dioxygen by copper is an important reaction in biological and industrial oxidation catalysis.[1−5] Consequently, the structure and reactivity of the products resulting from the reaction of discrete Cu(I) complexes with O_2 is of great interest. Many thermally sensitive products with dramatic structural variety result from this reaction.[4] This diversity of products results from the different reaction stoichiometries (**L**Cu^I:O_2) and the coordination mode of the reduced O_2 species, both of which are controlled by the ligand coordination environment. Typically, each **L**Cu(I) complex provides one electron ($1e^-$) in a reaction to give a Cu(II) species to which the reduced dioxygen species is ligated. Indeed, 1:1 Cu:O_2 superoxide complexes ([**L**$Cu^{II}(O_2^-)$]),[6,7] 2:1 peroxide complexes ([$\mathbf{L}_2(Cu^{II})_2(O_2^{2-})_2$]),[8,9] and 4:1 oxide level complexes ([$\mathbf{L}_4(Cu^{II})_4(O)_2$])[10] are products of the reaction of **L**Cu(I) and O_2.

Copper as a $1e^-$ reductant is also prevalent in biological copper systems. The binuclear copper proteins hemocyanin and tyrosinase reduce O_2 by $2e^-$, forming a [Cu(II)$_2$-μ-η^2:η^2-O_2^{2-}] peroxide-level complex.[1] In the multicopper oxidase enzymes such as laccase, $4e^-$ reduction of O_2 to an oxide-level (as water) requires four reduced copper centers. Three of the coppers form a trinuclear active site where the O_2 binds, and a fourth blue copper site, located 13 Å distant, provides the fourth reducing equivalent.[11] Substitution of the blue copper site by a redox innocent mercuric ion significantly impedes O_2 bond cleavage by the fully reduced trinuclear site. The absence of this fourth reducing equivalent stabilizes an intermediate in which dioxygen has been reduced by $2e^-$ to the peroxide level. A $3e^-$ reduced O_2 species is apparently not thermodynamically preferred, as the peroxide is ligated directly to an easily oxidized Cu(I) species.[12] These data support the notion that dioxygen bond cleavage in the native trinuclear enzymes occurs in two sequential $2e^-$ steps, with each of the four coppers providing $1e^-$.[13−15]

(1) Solomon, E. I.; Sundaram, U. M.; Machonkin, T. E. *Chem. Rev.* **1997**, *96*, 2563−2606.
(2) Klinman, J. P. *Chem. Rev.* **1996**, *96*, 2541−2562.
(3) Fox, S.; Karlin, K. D. *Dioxygen Reactivity in Copper Proteins and Complexes*; Fox, S., Karlin, K. D., Ed.; Blackie Academic & Professional: Glasgow, U.K., 1995; pp 188−231.
(4) Kitajima, N.; Moro-oka, Y. *Chem. Rev.* **1994**, *94*, 737−757.
(5) Tyeklár, Z.; Karlin, K. D. *Acc. Chem. Res.* **1989**, *22*, 241−248.
(6) Mahroof-Tahir, M.; Karlin, K. D. *J. Am. Chem. Soc.* **1992**, *114*, 7599−7601.
(7) Fujisawa, K.; Tanaka, M.; Moro-oka, Y.; Kitajima, N. *J. Am. Chem. Soc.* **1994**, *116*, 12079−12080.
(8) Jacobson, R. R.; Tyeklár, Z.; Farooq, A.; Karlin, K. D.; Liu, S.; Zubieta, J. *J. Am. Chem. Soc.* **1988**, *110*, 3690−3692.
(9) Kitajima, N.; Fujisawa, K.; Moro-oka, Y.; Toriumi, K. *J. Am. Chem. Soc.* **1989**, *111*, 8975−8976.
(10) Mukherjee, P.; Stack, T. D. P. Unpublished results.
(11) Messerschmidt, A.; Ladenstein, R.; Huber, R.; Bolognesi, M.; Avigliano, L.; Petruzzelli, R.; Rossi, A.; Finazzi-Agrò, A. *J. Mol. Biol.* **1992**, *224*, 179−205.
(12) Shin, W.; Sundaram, U. M.; Cole, J. L.; Zhang, H. H.; Hedman, B.; Hodgson, K. O.; Solomon, E. I. *J. Am. Chem. Soc.* **1996**, *118*, 3202−3215.
(13) Solomon, E. I.; Sundaram, U. M.; Machonkin, T. E. *Chem. Rev.* **1996**, *96*, 2563−2605.

S0002-7863(97)03545-2 CCC: $15.00
Published on Web 05/12/1998

Recently, the conventional expectation that **L**Cu(I) provides at most $1e^-$ in the redox reaction with O_2 has been challenged by two novel Cu/O_2 structural types formed at low temperature in aprotic solvents. These complexes display full O_2 bond cleavage even though their **L**Cu(I):O_2 stoichiometries are only 2:1[16−18] and 3:1,[19] respectively. These products are thermally sensitive and display characteristic spectroscopic features. Three examples of these 2:1 Cu:O_2 complexes have been crystallographically characterized as $[Cu_2(\mu\text{-}O)_2\mathbf{L}_2]^{2+}$ dimers.[16,18,20] The 2:1 form likely plays a significant role in Cu:O_2 chemistry, as it has been spectroscopically identified using a wide array of both diamine and triamine ligands. The Cu−O distances in the $[Cu_2O_2]$ planar rhombs are very short: for $([Cu_2(\mu\text{-}O)_2(Bn_3\text{-}(TACN))_2](SbF_6)_2)$, the average Cu−O distance is 1.81 Å,[18] and for $[Cu_2(\mu\text{-}O)_2L_2](CF_3SO_3)_2$, the average Cu−O distance is 1.80 Å, where L is *N*,*N*′-dimethyl-*N*,*N*′-diethyl-(1*R*,2*R*)-cyclohexanediamine.[16] Similar short Cu−O distances are observed in the solid-state material $KCu^{III}O_2$ (Cu−O = 1.84 Å).[21] The bond distances and overall 2+ charge on the dimer suggest a $[Cu^{III}_2O_2]^{2+}$ description of the core, though similarly short Cu−O distances are known for Cu(II) complexes.[7,8,22] Cu K-edge X-ray absorption spectroscopy, which directly probes the copper center, supports the Cu(III) oxidation state description.[23,24] The planar arrangement of the oxide ligands between the two copper centers facilitates the $2e^-$ oxidation of each copper center and full O_2 bond cleavage.″

This study concerns the second structural type which deviates from the common $1e^-$ Cu(I) redox reactivity. A 3:1 **L**Cu(I):O_2 stoichiometry leads to full O_2 bond cleavage consistent with $4e^-$ reduction of O_2 from three coppers. This 3:1 metal:O_2 stoichiometry is remarkable, as it is unprecedented not only for copper but for any metal. The asymmetric structure of the $[Cu_3O_2]^{3+}$ core (vide infra) suggests a mixed-valence cluster in which one copper center is more highly oxidized than the other two. Addressing the reason for this electronic asymmetry is the focus of this study.

$[Cu^I(MeCN)\mathbf{L}_{TM}]^+$, where $\mathbf{L}_{TM}$ is *N*,*N*,*N*′,*N*′-tetramethyl-(1*R*,2*R*)-cyclohexanediamine, reacts with O_2 in CH_2Cl_2 solution at −80 °C in a 3:1 Cu:O_2 stoichiometry. The crystal structure of the product, $[Cu_3(\mu\text{-}O)_2(\mathbf{L}_{TM})_3](CF_3SO_3)_3\cdot 4CH_2Cl_2$, is shown in Figure 1.[19] Two crystallographically independent $[Cu_3(\mu\text{-}O)_2(\mathbf{L}_{TM})_3]^{3+}$ cations, **1**·$(Tf)_3$ (Tf = CF_3SO_3), exist in the unit cell, each possessing crystallographically imposed 2-fold symmetry. Because the two cations are nearly isostructural (rms = 0.093 Å for the $[Cu_3(\mu\text{-}O)_2N_6]^{3+}$ cores), this study focuses on the single cation presented in Figure 1. The core atoms of

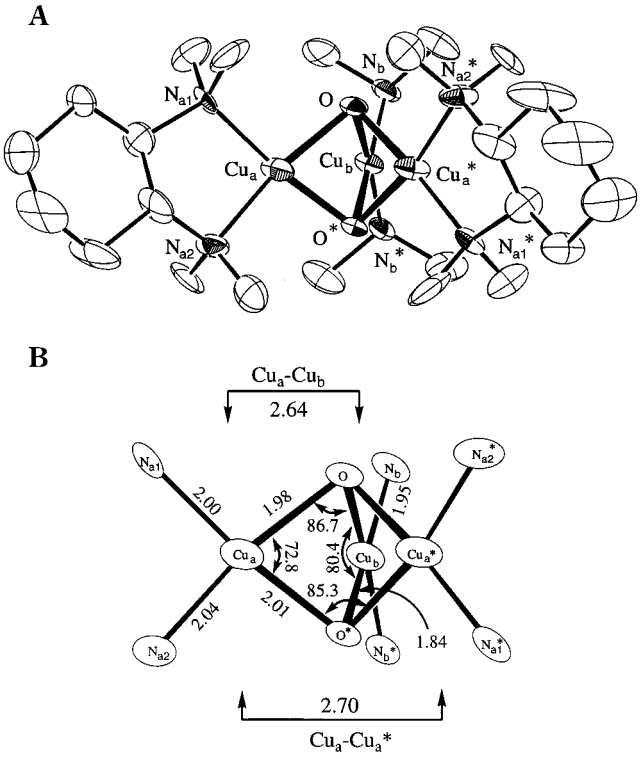

Figure 1. Crystal structure of **1**. (A) ORTEP representation (50% probability) of **1** with atom-labeling scheme. The view is nearly down the crystallographically imposed 2-fold axis on which Cu_b resides. The cyclohexyl ring carbon atoms attached to N_b and N_b* have been removed for clarity. (B) Expansion of core atoms with selected interatomic distances and angles.

1·$(Tf)_3$ are organized nearly in a trigonal bipyramidal arrangement but lack a 3-fold symmetry axis. A crystallographically imposed 2-fold axis passes through one of the three coppers, Cu_b, and bisects the vector between the two axially disposed oxygen atoms. The O−O vector is nearly normal to the copper plane. As $\mathbf{L}_{TM}$ is enantiopure (1*R*,2*R*), the symmetry of **1**·$(Tf)_3$ is C_2 rather than C_{2v}; the two copper atoms, Cu_a and Cu_a*, and two oxygen atoms, O and O*, are symmetry related (Figure 1), while Cu_b is unique.

The number of counteranions in the structure indicate that each trinuclear cluster is a 3+ cation. Each copper atom is coordinated in a square planar geometry consisting of two amine N atoms and the two bridging O atoms. The unique copper atom, Cu_b, has much shorter Cu−O and Cu−N bonds of 1.84 and 1.95 Å, respectively, than the symmetry equivalent Cu_a and Cu_a* atoms, which have average Cu_a−O and Cu_a−N bond lengths of 2.00 and 2.03 Å, respectively. The unusually short Cu_b−O distance of 1.84 Å, along with the short Cu_b−N bond lengths of 1.95 Å, suggests that Cu_b is more oxidized than Cu_a. Since all three copper ions are bridged by the same two μ_3-bridging O atoms, the observed inequivalence of the Cu−O bond lengths reflects oxidation state differences between the coppers. This supports the description of **1**·$(Tf)_3$ as a mixed valence $[Cu^{II}_2Cu^{III}]$ cluster. The distortion of the $[Cu_3(\mu\text{-}O)_2]$ core from D_{3h} geometry indicates that **1**·$(Tf)_3$ is strongly valence-trapped.

A description of the ground-state magnetism and electronic structure of the trinuclear complex **1**·$(Tf)_3$ is presented here. Magnetic circular dichroism (MCD) and magnetic susceptibility measurements determine the electronic ground spin state of **1**·$(Tf)_3$ and the energy splitting of the singlet and triplet states. Molecular orbital calculations provide an electronic structure description of this three-center, mixed-valence cluster. The

(14) Allendorf, M. D.; Spira, D. J.; Solomon, E. I. *Proc. Natl. Acad. Sci. U.S.A.* **1985**, *82*, 3063−3067.
(15) Spira-Solomon, D. J.; Allendorf, M. D.; Solomon, E. I. *J. Am. Chem. Soc.* **1986**, *108*, 5318−5328.
(16) Mahadevan, V.; Hou, Z.; Cole, A. P.; Root, D. E.; Solomon, E. I.; Lal, T. K.; Stack, T. D. P. *J. Am. Chem. Soc.* **1997**, *119*, 11996−11997.
(17) Tolman, W. B. *Acc. Chem. Res.* **1997**, *30*, 227−237 and references therein.
(18) Halfen, J. A.; Mahapatra, S.; Wikinson, E. C.; Kaderli, S.; Young, V. G., Jr.; Que, L., Jr.; Zuberbühler, A. D.; Tolman, W. B. *Science* **1996**, *271*, 1397−1400.
(19) Cole, A. P.; Root, D. E.; Mukherjee, P.; Solomon, E. I.; Stack, T. D. P. *Science* **1996**, *273*, 1848−1850.
(20) Mahapatra, S.; Young, V. G.; Kaderli, S.; Zuberbühler, A. D.; Tolman, W. B. *Angew. Chem., Int. Ed. Engl.* **1997**, *36*, 130−133.
(21) Hesterman, K.; Hoppe, R. *Z. Anorg. Allg. Chem.* **1969**, *367*, 249.
(22) Lee, S. C.; Holm, R. H. *J. Am. Chem. Soc.* **1993**, *115*, 11789−11798.
(23) DuBois, J.; Mukherjee, P.; Collier, A. M.; Mayer, J. M.; Solomon, E. I.; Hedman, B.; Stack, T. D. P.; Hodgson, K. O. *J. Am. Chem. Soc.* **1997**, *119*, 8578−8579.
(24) DuBois, J.; Mukherjee, P.; Solomon, E. I.; Stack, T. D. P.; Hedman, B.; Hodgson, K. O. *Stanford Synchroton Radiation Laboratory Report*, 1997.

localization and geometry of a mixed-valence system depend on the magnitudes of the electronic coupling between the ions and the vibronic trapping energy. These factors are discussed in the context of Jahn−Teller theory for this trinuclear cluster.

Experimental Section

Sample Preparation. Under an inert atmosphere, equimolar amounts of $[Cu(MeCN)_4](CF_3SO_3)$[25] (188 mg, 50 mmol) and *N*,*N*,*N*′,*N*′-tetramethyl-(1*R*,2*R*)-cyclohexanediamine, **L** (85 mg, 50 mmol), were dissolved in 10 mL of rigorously clean CH_2Cl_2 in a Schlenk flask.[19] Slow oxygenation was effected at −80 °C by purging dry O_2 over the initially colorless solution. Periodic agitation of the flask over 2 h was sufficient to ensure a homogeneous solution. Cold ether was layered over the resulting dark brown solution. After 4 days at −80 °C, brown microcrystalline product **1**·$(Tf)_3$ formed. The blue supernatant was decanted, and the residual brown solid washed with cold ether. The product is stable at −80 °C. Drying the sample under vacuum even at low temperature results in decomposition of the material.

Magnetic Circular Dichroism. MCD spectra were obtained using a JASCO J500C spectropolarimeter with an S-20 photomultiplier tube. The sample compartment was modified to accommodate an Oxford Instruments Spectromag 4 7T magnet dewar with optical windows. Solid samples suspended in ether were pipetted onto a quartz disk which was maintained at −80 °C under an ether bath. The sample was covered with a second quartz disk and ground between the two disks. Those samples that remained brown upon grinding were transferred immediately to the MCD dewar.

Magnetic Susceptibility. Magnetic susceptibility data were collected using a Quantum Design Model MPMS SQUID magnetometer. Between 1 and 8 mg of crystalline **1**·$(Tf)_3$ was loaded into the bottom half of a previously weighed gelatin capsule as an ether slurry at −80 °C. Excess ether was removed, and the top half of the of the gelatin capsule was inserted into the bottom half to form a pellet. The capsule was cooled in liquid nitrogen, and the two halves were secured with Kapton tape. The capsule was inserted into a plastic straw attached to the end of the sample rod and loaded into the SQUID magnetometer. The data were collected under both constant-field and variable-temperature conditions (1−5 T in linear 1/*T* increments from 2 to 40 K) and variable-field and variable-temperature conditions (1−5 T in linear 1/*T* increments from 1.8 to 30 K). After data collection, the sample was left to decompose at room temperature which allowed solvent evaporation. The capsule was weighed to determine the mass of the sample. Variable-temperature magnetic susceptibility measurements on the decomposed sample gave a nearly temperature-independent signal, precluding the need of a paramagnetic background correction. A correction for diamagnetism and temperature-independent paramagnetism was included as a parameter in the fit. Magnetic susceptibility data were fit using a least-squares Nealder−Mead simplex method implemented in Matlab.

Density Functional Calculations. Electronic structure calculations using the 1982 QCPE version of the Self-Consistent Field Xα Scattered Wave (SCF-Xα-SW) package[26−31] were run on DEC 3100 and IBM 3BT-RS/6000 computers. The exchange values, α, used in the atomic spheres are those of Schwarz[32] except in the case of H, for which an α of 0.777 25 was used.[33] The inter- and outer-sphere α values were

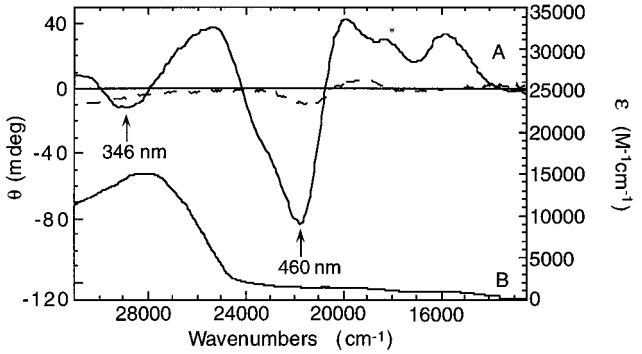

Figure 2. Magnetic circular dichroism (MCD) spectra of solid (—) **1** and its thermal decomposition product (- - -) at 1.6 K (top) and solution absorption spectrum of **1** in dichloromethane at 193 K (bottom). The asterisk indicates an MCD band with variable intensity in different sample preparations. The arrows indicate the peaks for which variable-field measurements were obtained.

the valence-electron weighted average of the atomic α values. Norman sphere radii were used for all atoms except copper. A copper sphere radius of 2.95 bohr was used rather than the Norman radius of ∼2.3 bohr, as it better reproduces the ground-state *g* values in $CuCl_4^{2-}$ and plastocyanin.[34,35] Calculations were repeated using several other Cu sphere radii ranging from the Norman value to 2.95 to gauge the effect of sphere radii on the results. The same orbital energy orderings are obtained with all choices of Cu sphere radii, but the energy splittings and wave functions varied with sphere radius. A Watson sphere with a radius equal to that of the outer sphere and charge equal but opposite to that of the model was included for ionic models unless otherwise noted. A relative change in the atomic potentials of less than 1×10^{-5} Rydbergs between iterations was used as a criterion for convergence. The coordinates of the models used for the SCF Xα-SW calculations are given in the Supporting Information.

LCAO density functional calculations were performed using the 2.0.1 version of the Amsterdam Density Functional (ADF) programs.[36] The Vosko−Wilk−Nusair local density approximation[37] for the exchange and correlation energy was used with the nonlocal gradient corrections of Becke and Perdew.[38,39] A triple-ζ Slater-type orbital (STO) basis set with a single-ζ STO polarization function was used for all atoms. Filled shell orbitals were treated by the frozen core approximation. Geometry optimizations were performed using the method of Ziegler et al.[40,41] provided in the ADF package.

Results and Analysis

Magnetic Circular Dichroism and Absorption. The mull MCD spectrum of **1**·$(Tf)_3$ at 1.6 K and 7 T are compared with the 193 K solution absorption spectrum (Figure 2). The MCD spectrum of the thermally decomposed product of **1**·$(Tf)_3$ under the same conditions exhibits little MCD intensity (Figure 2, top). The solid sample could not be finely ground due to its temperature sensitivity. Consequently, band intensities for energies above 27 000 cm^{-1} vary due to scattering, but the band positions are reproducible. The solution absorption spectrum (Figure 2, bottom) has an intense absorption peak at 355 nm (28 200 cm^{-1}) near the 346 nm (28 900 cm^{-1}) band in the mull MCD, suggesting that these bands correspond to the same transition. The magnetic field dependences from 0 to 7 T of

(25) Merrill, C. L.; Wilson, L. J.; Thamann, T. J.; Loehr, T. M.; Ferris, N. S.; Woodruff, W. H. *J. Chem. Soc., Dalton Trans.* **1984**, 2207−2221.
(26) Johnson, K. H.; Norman, J. G., Jr.; Connolly, J. W. D. *Computational Methods for Large Molecules and Localized States in Solids*; Plenum: New York, 1973.
(27) Slater, J. C. *The Self-Consistent Field for Molecules and Solids: Quantum Theory of Molecules and Solids*; McGraw-Hill: New York, 1974; Vol. 4.
(28) Connolly, J. W. D. *Semiempirical Methods of Electronic Structure Calculation, Part A: Techniques*; Plenum: New York, 1977.
(29) Cook, M. R. Ph.D. Thesis, Harvard University, 1981.
(30) Case, D. A. *Annu. Rev. Phys. Chem.* **1982**, *33*, 151−171.
(31) Cook, M.; Case, D. *QCPE Program #465* **1982**, *33*, 21−22.
(32) Schwartz, K. *Phys. Rev. B* **1972**, *5*, 2466−2468.
(33) Slater, J. C. *Int. J. Quantum Chem., Symp. No.7* **1973**, 533−544.
(34) Gewirth, A. A.; Cohen, S. L.; Schugar, H. J.; Solomon, E. I. *Inorg. Chem.* **1987**, *26*, 1133−1146.
(35) Gewirth, A. A.; Solomon, E. I. *J. Am. Chem. Soc.* **1988**, *110*, 3811−3819.
(36) te Velde, G.; Baerends, E. J. *J. Comput. Phys.* **1992**, *99*, 84−98.
(37) Vosko, S. H.; Wilk, L.; Nusair, M. *Can. J. Phys.* **1980**, *58*, 1200−1211.
(38) Becke, A. D. *Phys. Rev. Rev. A* **1988**, *38*, 3098−3100.
(39) Perdew, J. P. *Phys. Rev. B* **1986**, *33*, 8800−8802.
(40) Verluis, L. Ph.D. Thesis, University of Calgary, 1989.
(41) Fan, L.; Ziegler, T. *J. Chem. Phys.* **1991**, *95*, 7401.

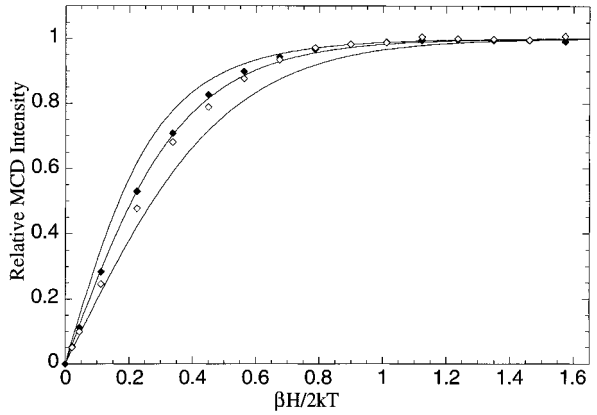

Figure 3. MCD intensity of 346 nm (◇) and 460 nm (◆) bands at 1.6 K as a function of magnetic field, normalized to the saturation limit. The Brillouin curves for $S = {}^3/_2$ (top curve), $S = 1$ (middle curve), and $S = {}^1/_2$ (bottom curve) normalized to their respective saturation limits are also shown.

the 346 and 460 nm MCD band intensities at 1.6 K, normalized to the maximum intensity at the high H/T limit, show similar saturation behavior (Figure 3). Superimposed on the data are Brillouin functions, $B_s(x)$, for $S = {}^1/_2$, $S = 1$, and $S = {}^3/_2$ spin systems normalized to the high-field saturation limit. $B_s(x)$ is given by

$$B_s(x) = \frac{2S+1}{2S}\coth\left(\frac{2S+1}{2S}x\right) - \frac{1}{2S}\coth\left(\frac{1}{2S}x\right) \qquad (1)$$

where $x = gS\beta H/kT$.[42] Comparison to the Brillouin functions shows that the MCD bands at 346 and 460 nm exhibit $S = 1$ saturation behavior. The band at 550 nm (18 200 cm^{-1}) is variable in the different sample preparations, indicating the presence of a temperature-sensitive paramagnetic impurity. This impurity disappears upon thermal decomposition of the sample. The reproducibility of all other bands including those at 346 and 460 nm clearly associate these bands with **1**·$(Tf)_3$. Since the saturation behavior can be selectively measured for the 346 and 460 nm bands, MCD is able to demonstrate that the trinuclear species has a triplet ground state, despite the presence of a paramagnetic impurity.

Magnetic Susceptibility. Magnetization saturation data for two separately prepared samples are shown in Figure 4. To determine the ground spin state, the magnetization saturation data were fit with eq 2:

$$M = NgS\beta B_s(x) \qquad (2)$$

where M is the magnetic moment, N is Avogadro's number, S is the spin of the complex, β is the Bohr magneton, and $B_s(x)$ is the Brillouin function given in eq 1. Thermal decomposition of **1**·$(Tf)_3$ produces a diamagnetic species having no temperature and field dependence. As these thermally sensitive samples could not be preweighed, the mass of the dried decomposed sample was used as the mass of the paramagnetic sample **1**·$(Tf)_3$. To account for any loss of the trinuclear species, the sample mass was permitted to vary in the data analysis. The data corresponds best with a spin state of $S = 1$ with an estimated upper limit of sample decomposition at 20%. The fit to the $S = {}^1/_2$, $S = 1$, and $S = {}^3/_2$ Brillouin functions, normalized to the saturation limit of the $S = 1$ fit, is presented in Figure 4. Though the MCD spectra reveal a variable amount of a temperature-sensitive paramagnetic impurity, inclusion of a $S = {}^1/_2$ impurity was not required to obtain a good fit to the magnetic susceptibility data. However, up to 15% of a $S = {}^1/_2$ impurity could be added with negligible loss of goodness of fit. The susceptibility data are highly reproducible and give the same $S = 1$ saturation behavior as the MCD data associated with specific electronic transitions of **1**·$(Tf)_3$.

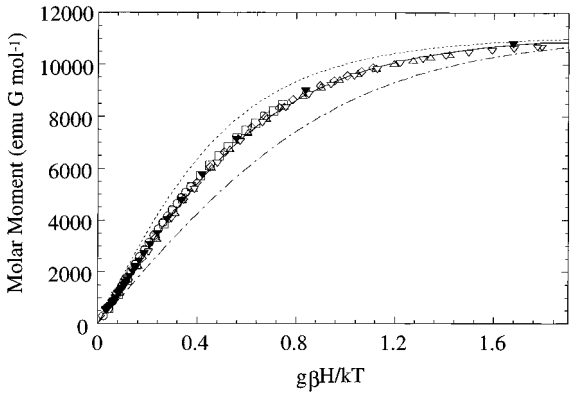

Figure 4. Molar magnetic moment plotted versus $g\beta H/kT$. Data were collected at magnetic fields of 1 T (○), 2 T (□), 3 T (◇), 4 T (△), and 5 T (▽ and ▼) over temperature ranges of 2−40 K linear in T (▼) and 1.8−30 K linear in $1/T$ (all others). The solid line is a fit of eq 2 to the data with $S = 1$. Also shown are the Brillouin functions for $S = {}^1/_2$ (- - -) and $S = {}^3/_2$ (- · -) normalized to the same saturation limit as the $S = 1$ fit.

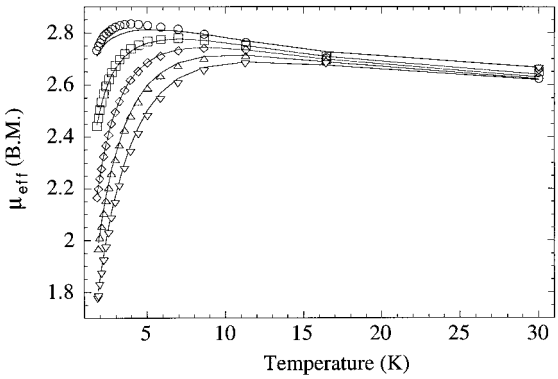

Figure 5. Effective magnetic moment (μ) plotted versus temperature for fields of 1 T (○), 2 T (□), 3 T (◇), 4 T (△), and 5 T (▽). Solid lines are calculated from a fit of the data to the modified Bleaney−Bowers expression given in eq 4 with $J = 7.0$ cm^{-1}.

Magnetic susceptibility data at five fields ranging from 1 to 5 T and temperatures ranging from 1.8 to 30 K are shown in Figure 5 plotted as μ_{eff} in Bohr magnetons versus temperature. These data were fit using the spin Hamiltonian

$$H = g\beta S_z' H_z - 2J\,\mathbf{S}_1\cdot\mathbf{S}_2 \qquad (3)$$

where $\mathbf{S}_1$ and $\mathbf{S}_2$ are the spins of the two Cu(II) centers of the trinuclear complex. This Hamiltonian leads to the following expression for μ_{eff}, in which c is a constant allowing for diamagnetism and temperature-independent paramagnetism.

$$\mu_{eff} = \left[\frac{\beta g T \sinh(g\beta H/kT)}{\beta H(\exp(-2J/kT) + 2\cosh(g\beta H/kT) + 1} + \frac{cT}{H}\right]^{1/2} \qquad (4)$$

This equation is a modification of the Bleaney−Bowers equation,[43] allowing for saturation. The fit to the data yields a value for the Heisenberg exchange coupling parameter, J, of

(42) Kahn, O. *Molecular Magnetism*; VCH Publishers: New York, 1993.

(43) Bleaney, B.; Bowers, K. D. *Proc. R. Soc. London* **1952**, *A214*, 451.

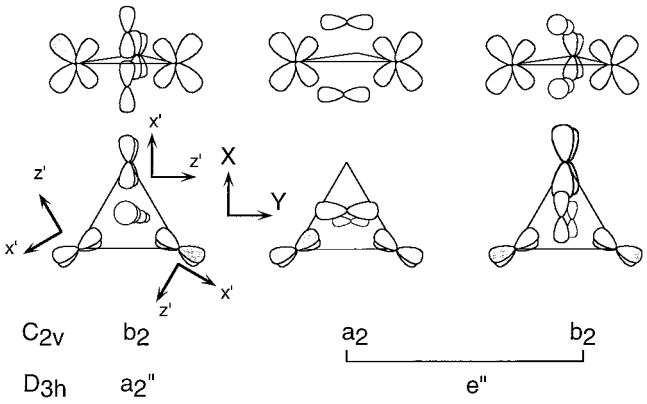

Figure 6. Symmetry-adapted valence orbitals for a D_{3h} bis-μ_3-oxo-bridged trinuclear copper complex with symmetry labels for C_{2v} and D_{3h} symmetry. The local symmetry axes used for the copper ions (x', y', z') and the molecular coordinate axes (X, Y, Z) used for the oxygen orbitals are also shown.

$+7.0$ cm^{-1}. Further analysis was attempted by adding the axial zero-field splitting term to the Hamiltonian:

$$H_{ZFS} = D[S_z^2 - {}^1/_3S(S+1)] \quad (5)$$

The best fit yielded a $|D|$ of 10^{-5} cm^{-1}, where $|D|$ is the energy splitting of the $S = \pm 1$ and $S = 0$ states at zero magnetic field. Reasonable fits could not be obtained for $|D| > 1.0$ cm^{-1}.

Molecular Orbital Calculations: Ground-State Electronic Structure and Magnetism. The valence orbitals of the [Cu_3-(μ-O)$_2$] core and the local coordinate axes used for each copper ion and the bridging oxygen atoms are shown in Figure 6. The symmetry of the [$Cu_3(\mu$-O)$_2$] core in complex **1**·(Tf)$_3$ is crystallographically C_2 (due to chirality of the ligands) but may be readily approximated as C_{2v} (Figure 1). The following calculations and discussion use an idealized model in which the bidentate *N*,*N*,*N*′,*N*′-tetramethyl-(1*R*,2*R*)-cyclohexanediamine ligand, $\mathbf{L}_{TM}$, is replaced by amines. The resulting ligand environment around each copper was flattened to achieve a square planar coordination geometry, resulting in C_{2v} molecular symmetry. As shown in Figure 6, the valence orbitals of the [$Cu_3(\mu$-O)$_2$] core consist of the linear combinations of the d_{xy} orbitals of the copper ions[44] which are antibonding with the p orbitals of the bridging oxygen atoms. The lobes of the Cu d_{xy} orbitals point directly at the O and N ligands. Six symmetry-adapted combinations of O p orbitals result from the two symmetry-equivalent O atoms. The three out-of-phase combinations of the p orbitals on the two oxygens (labeled O and O* in Figure 1), $p_{Ox}-p_{O*x}$, $p_{Oy}-p_{O*y}$, and $p_{Oz}-p_{O*z}$, have the appropriate symmetry (a_2 and b_2 representations) for bonding with the Cu d_{xy} orbitals. The orbitals depicted in Figure 6 are for the 3-fold symmetric D_{3h} limit in which all three copper ions are symmetry-equivalent.

In C_{2v} symmetry, the a_2'' and e'' orbitals of the D_{3h} model split into two b_2 orbitals and an a_2 orbital permitting the contribution of the unique copper ion in each MO to be different from that of the other two symmetry-equivalent copper ions. Note that in the C_{2v} model the *z*-axis is rotated by 90° from its orientation in the D_{3h} model. The reduction in symmetry allows the O p orbitals in the two b_2 molecular orbitals to mix with one another, rotating them within the plane of the unique copper and the oxygen atoms. The degree of localization of these C_{2v} molecular orbitals to the unique Cu_b or to the symmetry-related pair of Cu_a atoms defines the extent of valence trapping in this mixed-valence system.

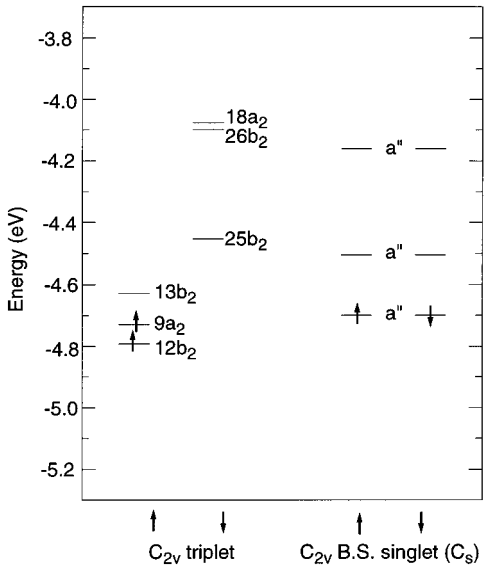

Figure 7. Energy level diagram for spin-unrestricted triplet (left) and broken-symmetry singlet (right) Xα-SW calculations on the C_{2v} trinuclear copper model.

Table 1. Valence Orbital Breakdown for the Spin-Unrestricted Triplet C_{2v} Calculation[a]

level	*E*/eV	occup.	Cu_b d	$Cu_{a/a*}$ d	O p total	O p_X (C_2)	O p_Y (a/a*)	O p_Z (O−O)
18 a_2	0.653	0 (−)	1	65	13	0	13	0
26 b_2	0.631	0 (−)	2	64	18	9	0	9
25 b_2	0.277	0 (−)	61	3	16	7	0	9
13 b_2	0.100	0 (+)	54	9	15	14	0	1
9 a_2	0.0	1 (+)	2	62	18	0	18	0
12 b_2	−0.062	1 (+)	10	54	18	2	0	16

[a] The last three columns give the O p orbital distribution where p_X is parallel to the molecular C_2 axis, p_Y is parallel to the $Cu_a-Cu_{a'}$ vector, and p_Z is parallel to the O−O vector as shown in Figure 6.

SCF-Xα-SW density functional calculations provide a quantitative description of the valence orbitals of the trinuclear copper complex. Energy level diagrams for the spin-unrestricted ground-state triplet and broken-symmetry singlet calculations are compared in Figure 7. The valence orbital composition of the spin unrestricted triplet calculation is given in Table 1. The spin-up levels corresponding to the three valence MO's (Figure 6) are the $12b_2$, $9a_2$, and $13b_2$ levels. The corresponding spin-down counterparts to these levels are $26b_2$, $18a_2$, and $25b_2$, respectively. A total of two electrons occupy these six one-electron valence orbitals. In the lowest energy triplet configuration, these electrons populate the $12b_2$ and $9a_2$ orbitals (Figure 7). The $12b_2$ and $9a_2$ orbitals are primarily composed of the antisymmetric and symmetric combinations (with respect to the C_2 symmetry axis) of the d_{xy} orbitals of the two symmetry-equivalent copper ions, Cu_a and Cu_a*. Figure 8 shows contour plots of these orbitals. The $9a_2$ and $12b_2$ orbitals contain relatively small contributions from the unique copper ion, Cu_b (2% and 10% respectively). The empty $13b_2$ spin-up LUMO orbital (Figure 8, top) is localized on Cu_b (54% on Cu_b versus 4% each on Cu_a and Cu_a*), consistent with the valence-trapped $Cu^{II}_2Cu^{III}$ description inferred from the crystal structure. The total charges on the copper ions were calculated using ADF rather than Xα-SW density functional calculations since the values obtained from Xα-SW calculations are very sensitive to the choice of Cu sphere radii. The gross charge for Cu_b is $+0.85$ e^- versus $+0.68$ e^- for Cu_a and Cu_a*. Although these charges are not expected to be quantitatively accurate, the significantly

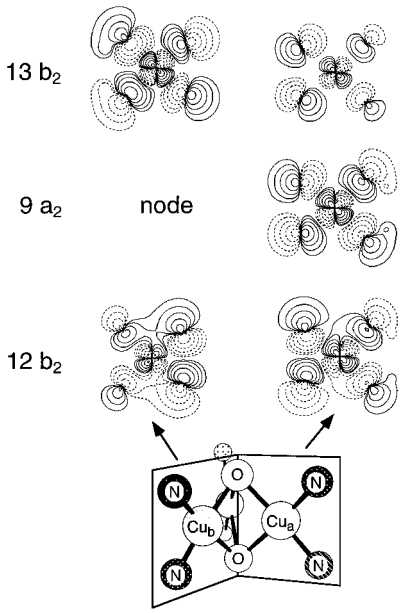

Figure 8. Xα-SW contour plots of the two highest occupied levels, $12b_2$ and $9a_2$, and the lowest unoccupied level, $13b_2$, for the spin-unrestricted triplet calculation. Two views of these orbitals are shown, one in the Cu_b-O-O plane (left) and one in the Cu_a-O-O plane (right).

greater positive charge on Cu_b does reflect a localization of the two valence electrons on Cu_a and Cu_a*.

The energy splitting of the singlet and triplet ground states can be calculated from the difference in the triplet high spin (E_{HS}) and broken-symmetry singlet (E_{BS}) total energies using the weak coupling approximation of Noodleman:[45]

$$-J = \frac{(E_{HS} - E_{BS})}{(S_{max})^2} \qquad (6)$$

where J is defined by the phenomenological Heisenberg Hamiltonian, $H = -2J\ \mathbf{S}_1\cdot\mathbf{S}_2$. ADF LCAO rather than Xα-SW density functional calculations were used to calculate the total energies for the triplet and broken-symmetry singlet states since ADF LCAO generally gives better values for the total energy. A triplet ground state is calculated with $2J = +878$ cm^{-1} in qualitative agreement with the experimentally observed ferromagnetic coupling. However, the calculated $2J$ value differs from the measured $2J$ of $+14$ cm^{-1} by over 860 cm^{-1}. A recent study on magnetic coupling constants in bis-hydroxo-bridged cupric dimers and in bis-alkoxo-bridged cupric dimers suggests that the level of calculation used here should predict the correct sign of the magnetic coupling, but may be in error by hundreds of cm^{-1} in the magnitude of J.[46] For weakly coupled cupric dimers, two electronic configurations can make significant contributions to the singlet ground state, whereas the triplet state has only one low-lying configuration. The broken-symmetry method permits localization of the one-electron orbitals to each side of the dimer and provides a better estimate of the singlet energy than can be obtained from a full-symmetry calculation using the single-determinant density functional approach. In the trinuclear complex, there are three energetically closely spaced valence levels (Figure 7) rather than the two in the dimer (vide infra), creating the possibility that the triplet state as well as the singlet state contains significant contributions from more than one configuration. This may contribute to the error in the calculated singlet−triplet splitting in the trinuclear complex.

The splitting of the valence orbitals of the trinuclear complex determines the ground-state electronic structure and magnetism of this trinuclear copper complex. Direct metal−metal interactions are negligible since the lobes of the d_{xy} valence orbitals are directed toward the ligands, not toward the adjacent copper ions which are separated by 2.64 Å ($Cu_a\cdots Cu_b$) and 2.71 Å ($Cu_a\cdots Cu_a$*). In $Cu_2(OAc)_4$, the Cu···Cu distance is 2.6 Å and there is no substantial metal orbital overlap.[47] Thus, in the trinuclear complex, the interactions of the Cu d_{xy} orbitals with the bridging oxo ligands and the nitrogen ligands determine the valence orbital splitting. The short Cu−O and Cu−N distances of Cu_b raise the energy of the $13b_2$ orbital localized on Cu_b relative to the $12b_2$ and $9a_2$ orbitals localized on Cu_a and Cu_a*. This results in the localization of the valence electrons on Cu_a and Cu_a* giving the unique copper, Cu_b, a higher oxidation state, Cu(III). The energy splitting of the singly occupied $12b_2$ and $9a_2$ orbitals (Figure 7) is of particular importance since these orbitals contain the two unpaired electrons. The energies of these orbitals will be referred to as ϵ_a and ϵ_s, respectively. The splitting of these orbitals is related to the singlet−triplet splitting according to the relationship[48]

$$2J = 2K_{ab} - \frac{(\epsilon_s - \epsilon_a)^2}{(J_{aa} - J_{ab})} \qquad (7)$$

where K_{ab} is an exchange integral giving the ferromagnetic contribution to the magnetic coupling and J_{aa} and J_{ab} are one-center and two-center Coulomb repulsion integrals, respectively. Equation 7 indicates that near-degeneracy of the valence orbitals, ϵ_a and ϵ_s, favors a triplet ground state and a large splitting of these orbitals favors a singlet ground state. In the spin-unrestricted triplet calculation on the C_{2v} trinuclear model, the small 0.06 eV (500 cm^{-1}) splitting between the singly occupied valence orbitals (Figure 7) is consistent with the observed and calculated ferromagnetism. The antibonding interactions of the d_{xy} orbitals with the amine and oxo ligands are very similar in the $12b_2$ and $9a_2$ orbitals, as expected given this near-degeneracy. The $12b_2$ and $9a_2$ orbitals both contain 18% O and have 16 and 15% N character, respectively. The very similar energies and oxo contributions of these orbitals indicate that the oxo orbitals do not mediate appreciable coupling between these Cu(II) ions. Another indication of the small oxo-mediated coupling between the copper ions is provided by the broken-symmetry singlet calculations. The spin-up and spin-down valence orbitals are highly localized to a single copper (Figure 9). In each orbital, there is a strong antibonding interaction between the oxo and one copper atom with little contribution from the second copper. This reflects a very weak antiferromagnetic superexchange pathway between the copper ions consistent with the observed ferromagnetism.

Molecular Orbital Calculations: Ground-State Geometry. The trinuclear complex is constructed from three equivalent **L**Cu subunits bridged by two μ_3-oxo ligands. In in the valence-

(44) The local coordinate axes for the copper ions were chosen to coincide with the symmetry axes of the idealized D_{3h} trimer. In these coordinates, the highest energy Cu d orbital is the d_{xy}. Using conventional axes for a monomeric square planar complex, this orbital would be labeled $d_{x^2-y^2}$.

(45) Noodleman, L. *J. Chem. Phys.* **1981**, *74*, 5737−5743.

(46) Ruiz, E.; Alemany, P.; Alvarez, S.; Cano, J. *J. Am. Chem. Soc.* **1997**, *119*, 1297−1303.

(47) Ross, P. K.; Allendorf, M. D.; Solomon, E. I. *J. Am. Chem. Soc.* **1989**, *111*, 4009−4021.

(48) Hay, P. J.; Thibeault, J. C.; Hoffman, R. J. *J. Am. Chem. Soc.* **1975**, *97*, 4884−4899.

Table 2. Crystallographic and Calculated Cu−O and Cu−N Bond Lengths and Difference between Calculated and Experimentally Derived C_{2v} or D_{3h} Distances (in Parentheses)

coordinates	Cu_b−O	Cu_a−O	Cu_b−N	Cu_a−N
crystallographic	1.83	1.995[a]	1.95	2.025[a]
C_{2v} ADF optimized	1.91 (+4%)	2.03 (+2%)	2.04 (+5%)	2.08 (+3%)
D_{3h} averaged x-tal	1.94		2.00	
D_{3h} ADF optimized	1.98 (+2%)		2.08 (+4%)	

[a] Average of two slightly inequivalent distances. This inequivalence is due to the slight distortion from C_{2v} symmetry.

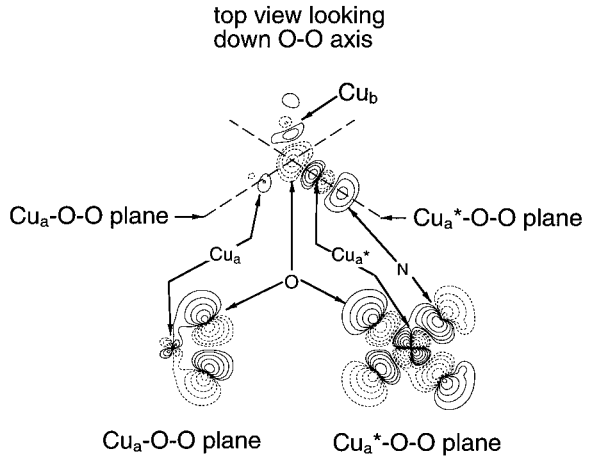

Figure 9. Xα-SW contours for the spin-up HOMO in the broken-symmetry singlet C_{2v} calculation. One contour (top) shows a slice parallel to the plane defined by the three Cu ions midway between the Cu plane and an O ligand. The other two views (bottom) show the planes containing either Cu_a or Cu_a* and the two O ligands.

delocalized limit a high-symmetry D_3 conformation of this molecule (differing from the crystal coordinates in that all Cu−O and Cu−N bond lengths are averaged over all three metals) would be the favored geometry. The observed C_2 conformation is the favored geometry for the valence-trapped limit. To consider the energetic stabilization accompanying the experimentally observed nuclear distortion and electron localization, ADF calculations were performed on the $[(LCu)_3(\mu\text{-}O)_2]$ model in D_{3h} as well as C_{2v} symmetry. The C_{2v} coordinates are derived from the crystallographic C_2 symmetry by adjusting the ligand environment about each copper to be planar and the O−O axis to be perpendicular to the plane defined by the three Cu centers (Cu_3 plane). These C_{2v}-symmetrized crystallographic coordinates were averaged over the three Cu sites to produce a model with D_{3h} symmetry. The total energies for the lowest triplet configuration of the C_{2v} and D_{3h} models were obtained from ADF density functional calculations. The C_{2v} model is more stable than the D_{3h} model by 5750 cm^{-1}. Thus, the calculations predict the crystallographically observed geometry to be strongly favored over the symmetrized, valence-delocalized geometry.[55]

The lowest energy D_{3h} geometry is not neccesarily that produced from averaging the C_{2v} coordinates. An additional a_1 Cu_2O_3 "breathing" distortion may increase or shorten all the Cu−O and Cu−N bond lengths relative to the average of the crystallographic coordinates in the lowest energy geometry. To account for this possibility, full geometry optimizations for the C_{2v} and D_{3h} models were performed using ADF density functional calculations. The core metrical parameters for the optimized structures are shown in Table 2. In the C_{2v} geometry-optimized structure, the Cu−O and Cu−N bond lengths are all increased from the crystallographically determined bond lengths by 2−5%, but the Cu_b−O and Cu_b−N distances remain substantially shorter than the symmetry equivalent Cu_a−O/Cu_a*−O and Cu_a−N/Cu_a*−N distances. The Cu−O and Cu−N bond lengths for the geometry-optimized D_{3h} structure are very close to the average over the three subunits of the C_{2v} geometry-optimized structure, lending justification to the choice of coordinates in the non-geometry-optimized D_{3h} model discussed. The difference in total energy between the triplet configurations for the C_{2v} and D_{3h} geometry-optimized models is 590 cm^{-1}.[55] The C_{2v} distortion is still favored by the calculation, but the stabilization energy for this distortion is significantly smaller than is calculated for the crystallographically derived C_{2v} coordinates and corresponding three-site-averaged D_{3h} coordinates. On the basis of the large magnitude of the C_{2v} distortion observed in crystal structure of the trinuclear complex, the larger 5800 cm^{-1} value for the vibronic stabilization energy calculated from the crystallographically derived coordinates is probably a more reasonable estimate.

Discussion

The crystal structure of the trinuclear copper complex **1**·$(Tf)_3$ shows that one of the three Cu ions has unusually short Cu−O bonds and that the complex has a 3+ charge. This dramatic asymmetry supports a description of **1**·$(Tf)_3$ as a valence-trapped $[Cu^{II}_2Cu^{III}(\mu\text{-}O)_2]$ cluster. In this description, the d^8 Cu(III) ion is low-spin and diamagnetic in this square planar anionic environment. Formulation of **1** as a trinuclear Cu(II) species, $[Cu^{II}_3(\mu_3\text{-}OH)(\mu_3\text{-}O)]$, is also consistent with an overall 3+ charge, assuming the additional proton is disordered over the two bridging oxygen atoms. Though X-ray crystallography is unable to differentiate between these two possibilities, the magnetic properties unambiguously support the mixed-valence composition. MCD and magnetic susceptibility data demonstrate that **1** has an $S = 1$ triplet ground state with a small ferromagnetic coupling constant of $J = +7.0$ cm^{-1}. This integer spin is only consistent with a mixed-valent trinuclear complex as the alternative all-Cu(II) composition requires an odd number of electrons on the cluster and a half-integer total spin.

The d^8 Cu(III) center in the trinuclear complex is stabilized by the square planar coordination geometry which concentrates the charged ligands in the plane of the single empty d_{xy} orbital. The 2− charge on the oxo ligands should also greatly stabilize

(49) Henson, M. J.; Solomon, E. I. Unpublished results.
(50) Burdett, J. K.; Seviv, S. *J. Am. Chem. Soc.* **1995**, *117*, 12788−12792.
(51) Crawford, V. H.; Richardson, H. W.; Wasson, J. R.; Hodgson, D. J.; Hatfield, W. E. *Inorg. Chem.* **1976**, *15*, 2107−2110.
(52) Charlot, M. F.; Jeannin, S.; Jeannin, Y.; Kahn, O.; Lucrece-Abaul, J.; Martin-Frere, J. *Inorg. Chem.* **1979**, *18*, 1675−1681.
(53) Charlot, M. F.; Kahn, O.; Jeannin, S.; Jeannin, Y. *Inorg. Chem.* **1980**, *19*, 1410−1411. A study of two such "butterfly" hydroxo-bridged cupric dimers concluded that increasing the dihedral angle between the two CuO_2 planes (while keeping the O···O and Cu−O distances constant) increases the antiferromagnetic interaction between the copper ions.
(54) Bersuker, I. B. *The Jahn−Teller Effect and Vibronic Interactions in Modern Chemistry*; Plenum Press: New York, 1984.
(55) Comparisons between total energies of C_{2v} and D_{3h} models were made with C_{2v} electronic symmetry imposed in the D_{3h} single-point calculations.[56]
(56) Bruyndonckx, R.; Daul, R.; Manoharan, P. T.; Deiss, E. *Inorg. Chem.* **1997**, *36*, 4251−4256.

the highly oxidized Cu(III) center. It is significant that the oxo valence orbitals are stabilized by interaction with the additional Cu centers both in the trinuclear complex and in the related $[RN_2Cu_2O_2]^{2+}$ oxo-bridged Cu(III) dimers. Xα-SW calculations on the trinuclear cluster show that the oxo and nitrogen ligands each contribute approximately 8% to the primarily Cu(III) d_{xy}-composed LUMO. A model consisting of the $[Cu^{III}(NH_3)_2(O)_2]$ fragment of the trinuclear model shows that without the stabilization from the two bridging Cu(II) ions, the calculated charge donation from oxo ligands increases to 32%. For oxo-bridged Cu(III) dimers, the charge donation from each oxo bridge to the pair of Cu(III) ions is calculated to be 9%,[49] very similar to that calculated for the trinuclear complex. Oxo-bridges also stabilize Cu(III) in the solid-state material $KCuO_2$.[50] Thus oxides appear to be very good ligands for stabilizing Cu(III) *when* the O^{2-} valence orbitals are sufficiently stabilized by bridging interactions with additional cations.

The localization of the two valence electrons to the two symmetry-equivalent Cu ions, Cu_a and Cu_a*, permits the magnetism of the trinuclear complex to be considered to arise only from the interaction of the two Cu(II) ions. The Cu(III) center could nevertheless indirectly affect the oxo-mediated interaction between the Cu(II) ions by its influence on the oxo orbitals. An Xα-SW calculation was performed on a bent $[((NH_3)_2Cu)_2(\mu\text{-}O)_2]$ dimer model identical to the C_{2v} model of the trinuclear complex except that the Cu(III) and its associated ammonia ligands have been removed. The splitting of the valence orbitals, ϵ_a and ϵ_s, is still very small in this bent dimer model, 0.01 eV compared to 0.06 eV in the trinuclear model. Ferromagnetic coupling is therefore predicted to persist even in the absence of the Cu(III) ion. The reduced $\epsilon_a-\epsilon_s$ splitting and associated superexchange interaction between the Cu(II) ions are therefore due to the bridging geometry of the $[Cu^{II}_2O_2]$ unit. The relationship between structural parameters and magnetic coupling in $[Cu^{II}_2X_2]$ dimers has been extensively studied for hydroxo, alkoxo, and halide bridges. On the basis of experimental studies of bis-hydroxo-bridged cupric dimers, a linear correlation between the $2J$ singlet−triplet splitting and the Cu−O−Cu bridging angle for these complexes is observed.[51] The antiferromagnetic coupling lessens as the Cu−O−Cu angle decreases, becoming ferromagnetic for Cu−O−Cu angles less than ∼98°. Hay, Thibeault, and Hoffmann relate this trend to the reduction in the splitting of the symmetric and antisymmetric combinations of the Cu(II) orbitals (eq 7) that occurs with decreasing Cu−O−Cu angle. The $[Cu^{II}_2O_2]$ unit in the trinuclear complex is very bent with a dihedral angle of 115° between the CuO_2 planes which gives a Cu−O−Cu angle of 85°. Simply flattening the $[Cu^{II}_2O_2]$ unit of the trimer while keeping O···O and Cu−O distances constant results in a Cu(II)−O−Cu(II) angle of 107°. This flattened complex has a calculated $|\epsilon_a-\epsilon_s|$ splitting of 0.34 eV and $2J = -2450$ cm^{-1}.[52,53] Lengthening O···O distance (with constant Cu−O) to give a Cu−O−Cu angle of 85° (Cu···Cu distance of 2.70 Å) gives $|\epsilon_a-\epsilon_s| = 0.08$ eV and $2J = +860$ cm^{-1}. The similarity between this result and that obtained for the trinuclear complex in which $|\epsilon_a-\epsilon_s| = 0.06$ eV and $2J = +878$ cm^{-1} indicates that the small Cu(II)−O−Cu(II) angle within the trinuclear cluster is responsible for the observed magnetic properties.

Distortion of the nuclear coordinates of the trinuclear mixed-valence system from the D_{3h} high-symmetry configuration is necessarily accompanied by a localization of the two valence electrons. The magnitude of this distortion is determined by two competing factors, the vibronic stabilization energy and the electronic delocalization energy. The latter is determined by the electronic coupling between the copper ions. The small ferromagnetic coupling of **1**·$(Tf)_3$ indicates that electronic coupling between the copper ions is weak. This weak coupling is corroborated by density functional calculations showing that the splitting between the symmetric and antisymmetric combination of the Cu d_{xy} orbitals is small in either C_{2v} symmetry (500 cm^{-1}) or the site-averaged D_{3h} symmetry (800 cm^{-1}). The weak ferromagnetic coupling takes place through the same oxo-bridge pathway that governs the electronic delocalization. Thus the energy associated with electronic delocalization in this molecule is expected to be small.

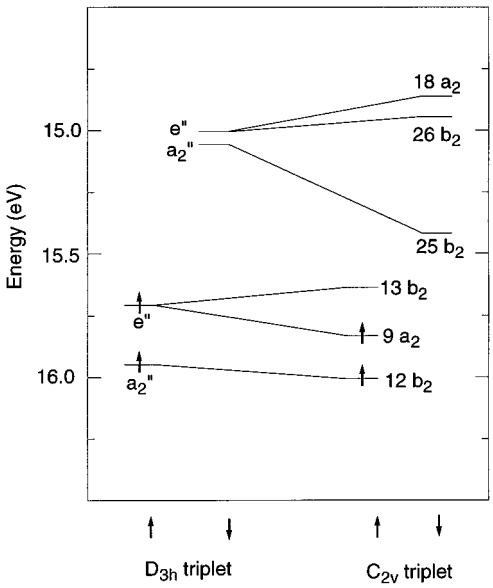

Figure 10. ADF energy level diagram for spin-unrestricted triplet calculations on the D_{3h} and C_{2v} models of **1** derived from crystallographic coordinates. This diagram shows the splitting and stabilization of the valence orbitals upon distortion from D_{3h} to C_{2v}.

In the high-symmetry D_{3h} limit, the triplet state of the trinuclear complex is a Jahn−Teller system. Figure 10 (left) shows the ADF molecular orbital energy diagram for the D_{3h}-symmetrized coordinates in which the crystallographic coordinates have been averaged over the three copper sites. The two valence electrons are in the a_2'' and e'' orbitals giving a $^3E'$ ground state and making this an [E′ ⊗ e′] Jahn−Teller (JT) system. The linear [E′ ⊗ e′] JT effect gives the well-known "Mexican hat" potential energy surface and a dynamic distortion.[54] The quadratic [E′ ⊗ e′] JT effect generates three minima in the "Mexican hat" potential and produces a static C_{2v} distortion. This potential surface as a function of Q_θ and Q_ϵ nuclear coordinates (the two components of the e′ vibration) is presented in Figure 11. The three minima in the Mexican hat potential correspond to distortions along linear combinations of these coordinates. One potential minimum is along the positive direction of the Q_θ mode and involves contraction of the square planar ligation at one Cu center and expansion by half the amount of the square planar ligation around the other two Cu's. The other two minima correspond to equivalent distortions rotated by 120° such that the contracted ligation is localized on each of the other two Cu's of the symmetric trimer. The correlation between the D_{3h} and C_{2v} orbitals of the trinuclear cluster is shown in Figure 10. The low-symmetry distortion splits the e″ orbitals, stabilizing the occupied orbital component of the e″ set. This is reflected in the 5800 cm^{-1} stabilization of the total energy. The computational models are for an isolated molecule and thus do not include crystal packing forces

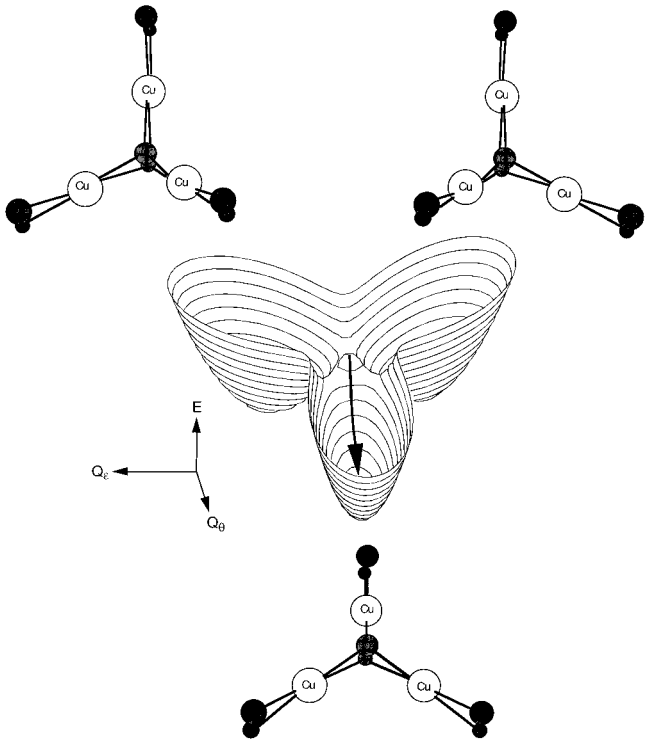

Figure 11. Lower sheet of the adiabatic potential energy surface for an E′ ⊗ e′ Jahn−Teller system with stong quadratic coupling as a function of distortions along the two components of the e′ mode, Q_θ and Q_ϵ. The arrow shows the experimentally observed C_{2v} distortion of the trinuclear copper complex. Structures for all three of the JT minima are also included.

that could contribute to the observed distorted structure. In addition, the calculation uses ammine ligands in place of the bulkier *N*,*N*,*N*′*N*′-tetramethylcyclohexanediamine ligands and thus removes intramolecular steric factors that could potentially also contribute to distortion. The ADF calculations nevertheless qualitatively reproduce the observed distortion of the trinuclear complex **1**·$(Tf)_3$ from 3-fold symmetry, indicating that observed C_{2v} distortion and valence-trapping is due to the Jahn−Teller stabilization of the C_{2v} $[Cu_3O_2]$ core.

In summary, the trinuclear cluster is a mixed-valence Cu(II,II,III) system. The extra hole is localized on the unique copper (giving Cu(III)) rather than on the oxo ligand due to the strong stabilization of the oxo valence orbitals which derives from the additional bridging interactions with the Cu(II)'s. The communication between d_{xy} orbitals on the Cu ions is weak as it involves superexchange through the oxo bridges which have approximately orthogonal orbital pathways to each copper. This leads to ferromagnetism between the two Cu(II)'s and weak electronic coupling between the Cu(III) and the Cu(II)'s. In the idealized D_{3h} high-symmetry limit which would be associated with complete electronic delocalization, the ground state is orbitally degenerate and subject to a large JT distortion toward the observed C_{2v} structure. This combination of large JT distorting force and a small electronic coupling between the coppers leads to the localization of the Cu(III) on one metal center.

Acknowledgment. The authors thank Thomas Brunold and Daniel Gamelin for useful discussions. This work was supported by grants from the National Institutes of Health: DK31450 (E.I.S.) and GM50730 (T.D.P.S.).

Supporting Information Available: Tables of Cartesian coordinates and input parameters for SCF-Xa-SW calculations and normal coordinate analysis (2 pages, print/PDF). See any current masthead page for ordering information and Web access instructions.

JA973545A